

CHARACTERIZING LOW-THRUST TRANSFERS FROM NEAR-RECTILINEAR HALO ORBITS TO LOW LUNAR ORBITS WITH Q-LAW

Yuri Shimane*, Dyllon Preston[†], and Koki Ho[‡]

Near rectilinear halo orbits (NRHOs) are an integral orbital regime in humanity's permanent return to cislunar space. Traffic between the NRHO and low-lunar orbit (LLO) is expected to increase dramatically, supporting cislunar activities. Linking NRHOs and LLOs via low-thrust transfers will be a vital piece of transportation infrastructure. This work provides an assessment of low-thrust transfers from NRHOs to LLOs using Q-law, a Lyapunov feedback controller based on Keplerian elements, treating the Earth as a third-body perturbation. Leveraging the deterministic nature of Q-law, low-thrust transfers between NRHOs and LLOs are characterized for various propulsion systems, spacecraft mass, and departure windows.

INTRODUCTION

Spearheaded by NASA's Artemis program, substantial efforts are directed toward the Moon. This is not limited to activities by traditional, space agencies and academia, but also extends to the numerous private companies working towards building a cislunar infrastructure, through projects such as the Commercial Lunar Payload Services (CLPS)¹ and LunaNet.² The Gateway, the first human outpost beyond low Earth orbit, will take a central role in upcoming cislunar exploration activities. Its nominal location, the 9:2 resonant L2 near-rectilinear halo orbit (NRHO), will see significant traffic, with both crew and cargo frequenting the Gateway architecture.³⁻⁸ The near-rectilinear halo orbit (NRHO) is of particular interest in the context of cislunar logistics as they provide a relatively stable orbit around the Moon with a constant line of sight with the Earth. Besides NRHOs, low lunar orbits (LLOs) are also critical locations for conducting activities in cislunar space. Crewed and robotic surface expeditions utilize LLOs before proceeding to their final descent to the target landing site. LLOs are also well-suited for science missions conducted from orbit due to their proximity to the lunar surface.

Transfers between NRHOs and LLOs will bare increasing importance as the infrastructure in the cislunar space continues to mature. The use of low-thrust propulsion for these transfers is particularly attractive for applications that do not involve crew; while low-thrust propulsion requires longer times of flight to accumulate enough control effort, rendering them unusable for typical crewed applications, the higher specific impulse results in significant propellant savings. These include the transportation of scientific equipment and cargo to and from the lunar surface, as well as more advanced concepts such as on-orbit servicing (OOS) or space tugs; for example, Astroscale, a Japanese

*PhD Candidate, School of Aerospace Engineering, Georgia Institute of Technology, GA 30332, USA

[†]Undergraduate Student, School of Aerospace Engineering, Georgia Institute of Technology, GA 30332, USA

[‡]Associate Professor, School of Aerospace Engineering, Georgia Institute of Technology, GA 30332, USA

OOS startup, announced last year its intentions to extend its activities in lunar environments,⁹ while Spaceflight, a US startup providing rideshare platforms and in-space transportation, has along its planned product lineups a vehicle capable of tugging payloads to cislunar space.¹⁰

The use of low-thrust propulsion for transfers in cislunar space has been studied by multiple authors; for example, Du and Starinova studied the use of low-thrust for orbit maintenance of NRHO under perturbations by solving the corresponding optimal control problem via the indirect method.⁸ A popular approach for constructing low-thrust transfers between libration point orbits involves “chaining” intermediate orbits to construct an initial guess as introduced by Pritchett et al,⁴ which is then solved via a direct method.¹¹ Pino and Howell¹² explores an energy-informed approach for providing these intermediate orbits in an adaptive manner. Das-Stuart et al¹³ considers a combination of periodic orbit databases and a graph-search approach to construct initial guesses that can then be corrected and/or optimized to actual flyable trajectories. Kayama et al looked at low-thrust transfers from a halo to an NRHO via successive convex optimization.¹⁴ In the context of transfers between NRHOs and LLOs, Horton et al¹⁵ have conducted an analysis for a high-powered SEP tug spacecraft application using NASA’s Copernicus software. Pino et al¹² and Park et al¹⁶ studied this problem for small spacecraft applications, such as the Lunar IceCube mission.

As highlighted by these works, low-thrust trajectory design in cislunar space remains difficult due to the complexity of the dynamics combined with the low control authority of the spacecraft. This makes optimizing a large number of transfers for various combinations of hyper-parameters prohibitive. To circumvent this challenge, this work employs Q-law, a Lyapunov controller developed in terms of two-body orbital elements,^{17–19} to generate large numbers of near-optimal NRHO-to-LLO transfers. Compared to traditional indirect and direct approaches for low-thrust trajectory optimization, Q-law is a feedback controller that can generate suboptimal transfers without the need for any open-loop optimization. Note that due to the fundamentally two-body nature of Q-law, this design strategy cannot be applied for transfers between libration point orbits, or transfers that involve an intermediate departure from the cislunar vicinity. Nonetheless, LLO can be defined in terms of Keplerian elements making it suitable for targeting with Q-law, and typical low-thrust transfers from NRHOs to LLOs may be conducted entirely within the cislunar regime, making Q-law an attractive technique for this application.

As a feedback controller, initial implementations of Q-law only included the capability to thrust at all times along the transfer. However, later implementations have incorporated heuristic-based coasting mechanisms,^{18,19} which allows for the spacecraft to choose to coast instead, if the application of thrust at a given angular position along its osculating orbit is deemed too unfavorable. While the resulting transfer is still suboptimal, this increases the solution space of transfers that can be obtained; arguably, a Q-law-based trajectory with no coasting is a sub-optimal proxy of a bang-bang, minimum time solution, while a trajectory with heuristic efficiency-based coasting is a sup-optimal proxy of a minimum mass solution.

The feedback form is especially useful when multiple low-thrust transfers must be designed within the scope of a single study. In the past, Q-law has been used in applications such as cislunar campaign logistics, trade-study for transferring from GTO to GEO, or debris removal mission designs.^{20–24} In the context of cislunar transfers, Jagannatha et al²⁵ utilized Q-law and invariant manifolds to design low-thrust transfers to Earth-Moon L1 periodic orbits. In Jagannatha et al²⁵ as well as in this work, while the control law is obtained assuming pure two-body dynamics, the perturbing effect of the Earth/Moon in the vicinity of the Moon/Earth is taken into account when applying the control and propagating the spacecraft’s state. In addition, the Moon’s J2 effects are

also included as a perturbing force. Thus, no simplifying compromise is made on the complexity of the dynamics itself.

In this work, low-thrust transfers from the Gateway’s NRHO to LLOs are studied. This application of Q-law in this context is distinguishable from other studies due to the strong influence of the third-body perturbation at the early stages of the transfer. This necessitates high duty ratios on the thrusters at the initial stages of the transfer in order to avoid being pulled away from the sphere of influence of the Moon. Meanwhile, once the spacecraft is within some sufficient vicinity from the Moon, a more economical coasting scheme may be more appropriate. To this end, we implement Q-law with efficiency parameters that can be switched at some point along the transfer. This enables the design via feedback control of transfers that can, in the first phase, aggressively apply control to head towards the target orbit, then later switch to a frugal phase, where the spacecraft may choose to coast more frequently.

We also devise a customized Runge-Kutta scheme that saves some of the expensive computation related to the decision on whether to thrust or coast at the first evaluation of the equations of motion. Furthermore, the integration is performed using an instantaneous Sundman transformation, thus achieving approximately constant steps in eccentric anomaly; this idea is similar to the piecewise Sundman transformation from Ottesen and Russel.²⁶ The resulting Q-law implementation is well-suited for exploring the considered trade space of low-thrust transfers from the NRHO to LLOs.

A multiobjective optimization problem minimizing both propellant and time of flight is constructed based on hyper-parameters of Q-law as well as departure location from the 9:2 resonant L2 NRHO. Multiple instances of this problem are solved for different values of spacecraft wet mass and thruster parameters.

DYNAMICAL SYSTEMS

This work considers two dynamical systems; firstly, the NRHO is constructed in the Earth-Moon circular restricted three-body problem (CR3BP). Then, the Gauss planetary equations with a third-body perturbation and thrust are used within the framework of Q-law. In this section, the CR3BP and the NRHO are first introduced. Then, the dynamics based on the Gauss planetary equations are discussed. Finally, the conversion process from the state vector in the CR3BP to the state vector in the Gauss planetary equations is shown.

Circular Restricted Three-Body Problem

The CR3BP equations of motion are commonly studied in the rotating frame; these are given by

$$\ddot{x} - 2\dot{y} = \frac{\partial U}{\partial x}, \quad \ddot{y} + 2\dot{x} = \frac{\partial U}{\partial y}, \quad \ddot{z} = \frac{\partial U}{\partial z} \quad (1)$$

Here, U is the pseudo-potential given by

$$U = \frac{x^2 + y^2}{2} + \frac{1 - \mu}{r_1} + \frac{\mu}{r_2} \quad (2)$$

where $\mu = M_2/(M_1 + M_2)$ is the mass ratio, and r_1, r_2 are the distances from the spacecraft to the two primary bodies

$$r_1 = \sqrt{(x + \mu)^2 + y^2 + z^2}, \quad r_2 = \sqrt{(x - (1 - \mu))^2 + y^2 + z^2} \quad (3)$$

In the context of the Earth-Moon system, the subscript $(\cdot)_1$ corresponds to the Earth and the subscript $(\cdot)_2$ corresponds to the Moon.

Near Rectilinear Halo Orbit The NRHOs are a subset of the halo orbit family, which exists as sets of periodic orbits revolving around any of the five libration points. They are distinguished from other members of halo orbits by their near rectilinear stability, characterized by stability indices $\nu_{\text{stb},i}$ defined by

$$\nu_{\text{stb},i} = \frac{1}{2} \left| \lambda_i + \frac{1}{\lambda_i} \right|, \quad i = 1, 2 \quad (4)$$

that is close to unity.^{27,28} Here, $\lambda \in \text{spec}(\Phi(P_{\text{NRHO}}, 0))$ where $\Phi(P_{\text{NRHO}}, 0)$ is the state-transition matrix over one period, also called the monodromy matrix. As indicated by the index i , the monodromy matrix for periodic orbits in the CR3BP has two reciprocal pairs of eigenvalues, resulting in two values of ν_{CR3BP} . From a practical perspective, NRHOs are attractive not only due to their stability but also due to the constant direct line of sight to the Earth, compared to other stable periodic orbits such as distant retrograde orbits (DRO).^{29,30}

Gauss Planetary Equations

The Gauss planetary equations for the Keplerian elements $\alpha = [a, e, i, \Omega, \omega, \theta]$ with respect to the Moon are given by

$$\dot{\alpha} = \mathbf{B} \mathbf{f} + \mathbf{D} \quad (5)$$

where

$$\mathbf{B} = \begin{bmatrix} \frac{2a^2 e \sin \theta}{h} & \frac{2a^2 p}{rh} & 0 \\ \frac{p \sin \theta}{h} & \frac{(p+r) \cos \theta + re}{h} & 0 \\ 0 & 0 & \frac{r \cos(\theta + \omega)}{h} \\ 0 & 0 & \frac{r \sin(\theta + \omega)}{h} \\ -\frac{p \cos \theta}{eh} & \frac{(p+r) \sin \theta}{eh} & -\frac{r \sin(\theta + \omega) \cos i}{h \sin i} \\ \frac{p \cos \theta}{eh} & -\frac{(p+r) \sin \theta}{eh} & 0 \end{bmatrix}, \quad \mathbf{D} = \begin{bmatrix} 0 \\ 0 \\ 0 \\ 0 \\ \frac{h}{r^2} \end{bmatrix}$$

The vector $\mathbf{f} = [f_r, f_t, f_n]$ are the radial, tangential, and normal components of the perturbing force acting on the Keplerian orbit. In this work, the perturbation comes from the spacecraft's low-thrust engine, \mathbf{f}_{LT} , the third-body perturbation of the Earth on the Moon-centered spacecraft orbit, \mathbf{f}_{\oplus} , and the J2 effect of the Moon, \mathbf{f}_{J2} ,

$$\mathbf{f} = \mathbf{f}_{\text{LT}} + \mathbf{f}_{\oplus} + \mathbf{f}_{\text{J2}} \quad (6)$$

To simplify the notation in (5), the following quantities have been defined as functions of the Keplerian elements

$$h = \sqrt{a\mu(1-e^2)}, \quad p = \frac{h^2}{\mu}, \quad r_p = a(1-e), \quad r = \frac{p}{1+e \cos \theta}$$

where μ is the gravitational parameter of the Moon.

Thrust Force The thrust force in the RTN frame for a thrust magnitude c_1 and spacecraft mass m is given by

$$\mathbf{f}_{LT} = \frac{\tau c_1}{m} \begin{bmatrix} \cos \beta \sin \alpha \\ \cos \beta \cos \alpha \\ \sin \beta \end{bmatrix} \quad (7)$$

where $\tau \in \{0, 1\}$ is the on/off throttle, α is the in-plane, and β is the out-of-plane angle of the thrust vector in the RTN frame. In addition to the six orbital elements, the mass of the spacecraft is propagated with the equation

$$\dot{m} = -\tau c_2 \quad (8)$$

where $c_2 = c_1/(g_0 I_{sp})$ is the mass-flow rate of the engine.

Thrid-Body Perturbation The third-body perturbation force in the RTN frame is given by

$$\mathbf{f}_{\oplus} = \mu_{\oplus} \left(\frac{\mathbf{r}_{\oplus} - \mathbf{r}}{\|\mathbf{r}_{\oplus} - \mathbf{r}\|^3} - \frac{\mathbf{r}_{\oplus}}{\|\mathbf{r}_{\oplus}\|^3} \right) \quad (9)$$

where $\mathbf{r} = [r, 0, 0]$ is the position of the spacecraft in RTN frame, and \mathbf{r}_{\oplus} is the position of the Earth in the RTN frame, given by

$$\mathbf{r}_{\oplus} = a_{\oplus} \begin{bmatrix} \cos \tilde{\theta} \cos (\lambda_{\oplus} - \Omega) + \cos i \sin \theta \sin (\lambda^{\Omega} - \Omega) \\ -\sin \tilde{\theta} \cos (\lambda_{\oplus} - \Omega) + \cos i \cos \theta \sin (\lambda_{\oplus} - \Omega) \\ -\sin i \sin (\lambda_{\oplus} - \Omega) \end{bmatrix} \quad (10)$$

where $\tilde{\theta} = \omega + \theta$ is the argument of latitude, a_{\oplus} is the semimajor axis of the Moon's orbit about the Earth, μ_{\oplus} is the gravitational parameter of the Earth, and λ_{\oplus} is the angular position of the Earth with respect to the inertial x -axis of the Moon-centered frame. This angle is time-dependent with the motion of the Earth and is given by

$$\lambda_{\oplus} = \lambda_{\oplus,0} + n_{\oplus} t \quad (11)$$

where $\lambda_{\oplus,0}$ is the initial angular position.

J2 Effect The J2 effect in the RTN frame is given by³¹

$$\mathbf{f}_{J_2} = \frac{3\mu J_2 R_e^2}{2r^4} \begin{bmatrix} 3 \sin^2 i \sin^2 \tilde{\theta} - 1 \\ -\sin^2 i \sin 2\tilde{\theta} \\ -\sin 2i \sin \tilde{\theta} \end{bmatrix} \quad (12)$$

where J_2 is the J2 coefficient, R_e is the reference radius of the body, and $\tilde{\theta}$ is the argument of latitude with the same definition as in equation (10).

Conversion from CR3BP to Keplerian Elements

The state vector of the NRHO in the CR3BP must be converted to Keplerian elements to be propagated with the Gauss planetary equations. We first discuss the canonical scales used in the two representations of the dynamical system, then present the procedure for converting from the CR3BP representation to the Gauss planetary equations representation.

Table 1. Canonoical scales for the CR3BP and the Gauss planetary equations

Parameter	CR3BP (C)	Gauss planetary equations (G)
Length unit LU, km	$3.847479920112920 \times 10^5$	1738
Time unit TU, s	$3.756998590849907 \times 10^5$	1034.5587359766118
Earth gravitational parameter μ_{\oplus}	0.98784941573006	81.26410601427115
Moon gravitational parameter μ	0.012150584269940354	1.0
System angular rate n_{\oplus} , rad/TU	1.0	0.0027369035713274096

Canonical Scales The use of canonical scales is prevalent in astrodynamics to avoid numerical difficulties. In the CR3BP, the mass is normalized such that the gravitational parameters of the two celestial bodies add up to unity. This is useful as the rotational speed of the system, n_C , becomes unity as well. Then, the canonical unit for time can naturally be defined such that the CR3BP system's period $P_{\text{CR3BP}} = 2\pi \times \text{TU}_C$, leading to the canonical length unit being the semi-major axis of the CR3BP system.

While this definition is useful for integrating the CR3BP equations of motion (1), it is preferable to have a different set of scales for integrating motions near the Moon, such as for LLOs, with the Gauss planetary equations (5). This is particularly important for numerical stability using Q-law, which we will introduce in the subsequent Section. As such, we define a different set of canonical scales for working with equation (5). Specifically, we define the gravitational parameter of the Moon to be unity and set the length unit LU_G to coincide with the lunar radius. Then, the time unit follows that the period of a hypothetical lunar circular orbit with a radius equal to the lunar radius $P_{\text{Lunar radius}} = 2\pi \times \text{TU}_G$. These canonical scales are summarized in Table 1.

Conversion Procedure The conversion from CR3BP to Keplerian elements first involves converting the state in the Earth-Moon rotating frame to the Moon-centered inertial frame, then converting the inertial state to Keplerian elements with respect to the Moon. In particular, given the Cartesian state $\mathbf{x}_{\mathcal{R}}(t) \in \mathbb{R}^6$ of the NRHO at time $t_0 \in [0, P_{\text{NRHO}}]$, the following four operations are to be conducted:

1. Shift center from the Earth-Moon barycenter to the Moon by subtracting $[1 - \mu, 0, 0, 0, 0, 0]$
2. Convert Cartesian state in the rotating frame $\mathbf{x}_{\mathcal{R}}$ to a Cartesian state in the inertial frame $\mathbf{x}_{\mathcal{I}}$ via the transformation

$$\mathbf{x}_{\mathcal{I}} = \mathbf{C}(\psi)\mathbf{x}_{\mathcal{R}} = \begin{bmatrix} \cos \psi & -\sin \psi & 0 & 0 & 0 & 0 \\ \sin \psi & \cos \psi & 0 & 0 & 0 & 0 \\ 0 & 0 & 1 & 0 & 0 & 0 \\ -n_C \sin \psi & -n_C \cos \psi & 0 & \cos \psi & -\sin \psi & 0 \\ n_C \cos \psi & -n_C \sin \psi & 0 & \sin \psi & \cos \psi & 0 \\ 0 & 0 & 0 & 0 & 0 & 1 \end{bmatrix} \mathbf{x}_{\mathcal{R}} \quad (13)$$

where $\psi = \psi_0 + n_C t_0$, where t_0 is in TU_C

3. Re-scale position by LU_C/LU_G and velocity by $(\text{LU}/\text{TU})_C/(\text{LU}/\text{TU})_G$

4. Convert Cartesian state to Keplerian elements using μ_G , and set

$$\lambda_{\oplus,0} = \pi + n_G \left(t_0 \frac{\text{TU}_C}{\text{TU}_G} \right) \quad (14)$$

ORBIT TRANSFER DESIGN WITH Q-LAW

While Q-law may be defined in any arbitrary orbital elements, we use the formulation based on the Keplerian elements in this work. This choice would not be appropriate if an inclination close to $i = 0$ or $i = \pi$ is likely to occur during the transfer due to the $\sin i$ terms in denominators of the Gauss planetary equations (5). However, the NRHO has its apse largely along the pole of the Moon, and LLOs of interest are typically near-polar, with $i \approx \pi/2$; hence, the $\sin i$ -singularities are unlikely to occur during the transfer. Meanwhile, the singularity for $e = 0$ is avoided by setting a tolerance on the final target LLO's e at some small value above 0.

As shown in equations (5), the Keplerian dynamics of the spacecraft is propagated with both the thrust force f_{LT} as well as the third-body perturbation f_{\oplus} and the J2 effect of the Moon f_{J2} . Note however that the controller is only exposed to the pure Keplerian dynamics, and the thrust vector f_{LT} is deduced assuming no other perturbations are acting on the spacecraft.

In this section, Q-law is discussed in two-fold; first, the Lyapunov function which is at the core of the controller is introduced. Then, the efficiency-based coasting mechanism by Petropoulos¹⁹ is presented. Finally, the procedure for implementing Q-law in the context of the transfer in the cislunar region is discussed.

Lyapunov Function

Let the five slow Keplerian elements excluding θ be expressed as $\tilde{\alpha} = \{a, e, i, \Omega, \omega\}$. The Lyapunov function for the controller is given by

$$Q = (1 + W_p \Theta_p) \sum_{\tilde{\alpha}} S_{\tilde{\alpha}} W_{\tilde{\alpha}} \left(\frac{\tilde{\alpha} - \tilde{\alpha}_T}{\dot{\tilde{\alpha}}_{xx}} \right)^2 \quad (15)$$

where α is the osculating elements of the spacecraft and $\tilde{\alpha}_T$ is the targeted elements. Note that Q essentially quantifies the separation of the osculating slow orbital elements of the spacecraft from the desired orbital elements from the numerator $\tilde{\alpha} - \tilde{\alpha}_T$. The denominator $\dot{\tilde{\alpha}}_{xx}$ represents the maximum achievable rate of change of each orbital element on the osculating orbit. Expressions for $\dot{\tilde{\alpha}}_{xx}$ are given in Petropoulos.¹⁹

Element-wise, each orbital element difference is multiplied by a weight $W_{\tilde{\alpha}}$. If only some of the elements need to be targeted, the weight $W_{\tilde{\alpha}}$ corresponding to the negligible element may be set to 0; for example, if a circular orbit with $e = 0$ is to be targeted, the weight for the argument of periapsis W_{ω} may be set to 0. In addition, the $S_{\tilde{\alpha}}$ is an additional scaling factor given by

$$S_{\tilde{\alpha}} = \begin{cases} \left[1 + \left(\frac{|a - a_T|}{\sigma a_T} \right)^{\nu} \right]^{1/\zeta}, & \tilde{\alpha} = a \\ 1, & \text{otherwise} \end{cases} \quad (16)$$

where σ , ν and ζ are scalar coefficients; the role of $S_{\tilde{\alpha}}$ is to prevent converging towards $a \rightarrow \infty$.

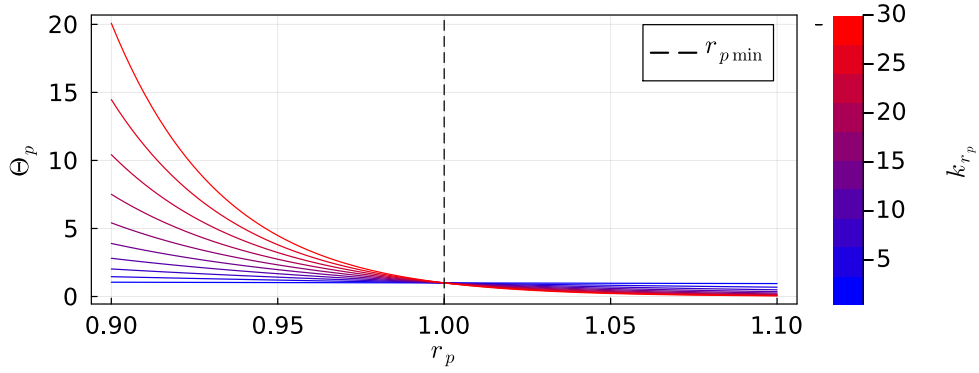


Figure 1. Periapsis penalty function Θ_p against periapsis r_p with $r_{p \min} = 1$

Outside the sum, Θ_p is a penalty term on the periapsis, multiplied by the scalar weight W_p , and is given by

$$\Theta_p = \exp \left[k_{r_p} \left(1 - \frac{r_p}{r_{p \min}} \right) \right] \quad (17)$$

Effectively, this imposes a penalty on the periapsis radius r_p against a user-defined, minimum allowed radius $r_{p \min}$. While the weight W_p simply scales the relative importance placed on the minimum periapsis, k_{r_p} tunes the sensitivity of this penalty with respect to how close the osculating r_p is to the threshold $r_{p \min}$. This is illustrated in Figure 1, where the penalty Θ_p increases at a faster rate for larger k_{r_p} .

Applying Lyapunov stability theory in the control context and assuming full throttle such that $\tau = 1$, we seek the optimal control angles α^* and β^* such that

$$[\alpha^*, \beta^*] = \underset{\alpha, \beta}{\operatorname{argmin}} \dot{Q} \quad (18)$$

Expressing \dot{Q} in terms of α and β ,

$$\dot{Q} = D_1 \cos \beta \cos \alpha + D_2 \cos \beta \sin \alpha + D_3 \sin \beta \quad (19)$$

where

$$D_1 = \sum_{\alpha} \frac{\partial Q}{\partial \tilde{\alpha}} \frac{\partial \tilde{\alpha}}{\partial f_t}, \quad D_2 = \sum_{\alpha} \frac{\partial Q}{\partial \tilde{\alpha}} \frac{\partial \tilde{\alpha}}{\partial f_r}, \quad D_3 = \sum_{\alpha} \frac{\partial Q}{\partial \tilde{\alpha}} \frac{\partial \tilde{\alpha}}{\partial f_n} \quad (20)$$

Expressions for $\partial Q / \partial \tilde{\alpha}$, while cumbersome, may be obtained with ease through the use of a symbolic toolbox. Meanwhile, $\partial \tilde{\alpha} / \partial f_r$, $\partial \tilde{\alpha} / \partial f_t$, and $\partial \tilde{\alpha} / \partial f_n$ are simply column vectors consisting of the first 5 entries of each column in matrix \mathbf{B} from equation (5). Differentiating equation (19) with respect to α and β and setting the system to zero, the optimal angles are given by

$$\alpha^* = \arctan(-D_2, -D_1) \quad (21)$$

$$\beta^* = \arctan \left(\frac{-D_3}{\sqrt{D_1^2 + D_2^2}} \right) \quad (22)$$

Note that α^* is found via the four-quadrant arc-tangent function in the range $[-\pi, \pi]$, while β^* is found via the normal arc-tangent function in the range $[-\pi/2, \pi/2]$.

It is worthwhile to consider what type of solution a transfer with $\tau = 1$ at all times represents; from classical analysis of optimal control theory, it is known that the optimal solution to a minimum-time problem requires a bang-bang control profile making use of the control at all times; thus, a $\tau = 1$ solution is a suboptimal feedback-controlled analog of a minimum-time transfer.

Coasting Mechanism

The mechanism for coasting is based on two quantities, η_a and η_r , representing the absolute and relative effectiveness of applying the thrust at the current location on the osculating orbit. These are given by

$$\eta_a = \frac{\dot{Q}_n}{\dot{Q}_{nn}} \quad (23)$$

$$\eta_r = \frac{\dot{Q}_n - \dot{Q}_{nx}}{\dot{Q}_{nn} - \dot{Q}_{nx}} \quad (24)$$

where

$$\dot{Q}_n = \min_{\alpha, \beta} \dot{Q} \quad (25)$$

$$\dot{Q}_{nn} = \min_{\theta} \left(\min_{\alpha, \beta} \dot{Q} \right) \quad (26)$$

$$\dot{Q}_{nx} = \max_{\theta} \left(\min_{\alpha, \beta} \dot{Q} \right) \quad (27)$$

The minimum \dot{Q} for a given θ , \dot{Q}_n , is computed by obtaining the optimal angles α^* and β^* from equations (21) and (22), and substituting them back to equation (19). Computing the exact values of \dot{Q}_{nn} and \dot{Q}_{nx} via minimizing against θ are impractical; instead, \dot{Q}_n is computed over N_θ points along the orbit, and the minimum/maximum values are taken as approximations of \dot{Q}_n and \dot{Q}_{nx} , respectively. While increasing N_θ would result in more accurate approximations, the computation of \dot{Q}_n is costly and should not be conducted too many times.

By setting cut-off effectiveness thresholds $\eta_{a \min}$ and $\eta_{r \min}$, the throttle τ is chosen such that

$$\tau = \begin{cases} 1 & \eta_a \geq \eta_{a \min} \text{ and } \eta_r \geq \eta_{r \min} \\ 0 & \text{otherwise} \end{cases} \quad (28)$$

Effectively, this formulation enables the control to be applied only at locations along the orbit where the relative and absolute efficiency of thrusting at that θ is beyond the predefined thresholds. Again, referring to optimal control theory, thrust profiles involving only full-throttle arcs with $\tau = 1$ and coasting arcs with $\tau = 0$, or a so-called bang-off-bang strategy, arise as solutions to mass-optimal problems. As such, a Q-law solution with coasting may be understood as a suboptimal feedback-controlled analog of a minimum-mass transfer.

Two-Stage Efficiency Scheme In some applications, modifying the efficiency along the transfer may be desirable. For example, in the context of NRHO to LLO transfers, the earlier half of the transfer necessitates more thrusting effort to reduce the spacecraft energy before being perturbed

out of the lunar sphere of influence, while the latter half may be able to accept a more reserved thrusting strategy, with higher values of $\eta_{a \min}$ and/or $\eta_{r \min}$. To this end, we implement a two-stage efficiency scheme, where an energy threshold-based switch is used to alter the values of $\eta_{a \min}$ and $\eta_{r \min}$. This variant of Q-law thus requires a pair of efficiency thresholds $\eta_{a \min, i}$ and $\eta_{r \min, i}$ for $i = \{1, 2\}$, such that

$$[\eta_{a \min} \quad \eta_{r \min}] = \begin{cases} \begin{bmatrix} \eta_{a \min, 1} & \eta_{r \min, 1} \end{bmatrix} & \mathcal{E} \geq \mathcal{E}_{\text{thres}} \\ \begin{bmatrix} \eta_{a \min, 2} & \eta_{r \min, 2} \end{bmatrix} & \mathcal{E} < \mathcal{E}_{\text{thres}} \end{cases} \quad (29)$$

We note that, ideally, it is desirable to adjust the efficiency as a function of, for example, the current states and targeted states. This is the idea behind the reinforcement learning agent trained in Holt et al.²³ In the scope of this work, we prefer to maintain a low number of parameters in favor of development and implementation speed. The two-stage efficiency scheme is thus a compromise to achieve the desired complexity of the coasting mechanism with a minimal number of parameters.

Customization of Integration Scheme

The previously discussed dynamics and feedback control law are numerically integrated to yield transfers. At this point, we would bring our attention to two critical aspects of this process: the speed and stability of the numerical integration. We note that, for the sake of speed, variable time-step integrators are typically suited for reducing the integration time while also maintaining the error under a user-defined threshold; however, for the sake of numerical stability, the feedback controller along with the discrete nature of the throttle (28) makes them inadequate.

To tackle these challenges, two modifications are made to a naive integration scheme. Firstly, the computational cost of a single integration step is reduced by limiting the evaluation of \dot{Q}_n from equation (25) to be done only once across N_θ points. Secondly, a piecewise Sundman transformation is leveraged in order to determine step sizes that are fixed in anomaly angle, resulting in variable time steps without the need for a higher-order correction step. Figure 2 illustrates these two modifications, adopted to a 4th order Runge-Kutta scheme.

Economic Runge-Kutta Scheme for Computation of the Efficiencies Runge-Kutta schemes involve evaluating the equations of motion multiple times over each iteration. For example, a 4th order Runge-Kutta scheme (RK4) requires 4 evaluations of the equations of motion, such that the state at step k is updated via

$$\mathbf{x}_{k+1} = \mathbf{x}_k + \frac{1}{6} (\mathbf{k}_1 + 2\mathbf{k}_2 + 2\mathbf{k}_3 + \mathbf{k}_4) \quad (30)$$

where \mathbf{k}_1 through \mathbf{k}_4 are the well-known four evaluations of the equations of motion for RK4. The main computational cost of $d\mathbf{x}/dt$ in Q-law comes from the N_θ evaluations of \dot{Q}_n to obtain approximate expressions of \dot{Q}_{nn} and \dot{Q}_{nx} . With RK4, this amounts to $4N_\theta$ evaluation of \dot{Q}_n .

Assuming the elements vary only slowly, the values of \dot{Q}_{nn} and \dot{Q}_{nx} are nearly constant between two successive steps in the integration. With this assumption, it is possible to reduce the computational cost of integrating the equations of motion by saving and reusing \dot{Q}_{nn} and \dot{Q}_{nx} . Thus, using RK4 as an example, while the evaluation of \mathbf{k}_1 requires N_θ evaluations of \dot{Q}_n to determine whether to thrust or coast according to equation (28), the remaining evaluations of \mathbf{k}_2 , \mathbf{k}_3 , and \mathbf{k}_4 each require at most a single evaluation of equation (18) to obtain the thrust angles, if thrust is applied at the considered integration step.

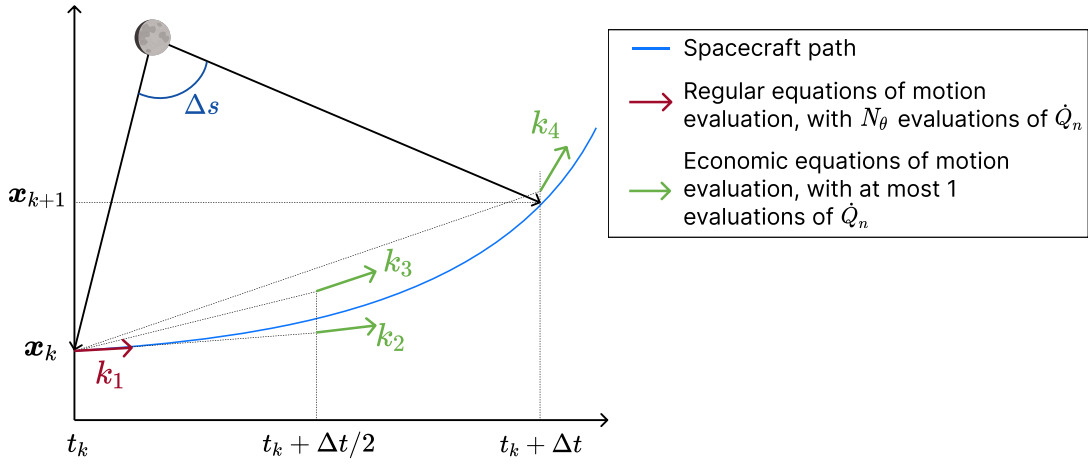


Figure 2. Custom integration based on 4th order Runge-Kutta scheme, with economic evaluation of the equations of motion and fixed angle-based step size Δs .

Supposing again that the integration is done with RK4, this amounts to N_θ evaluations when $\tau = 0$, or $N_\theta + 3$ evaluations when $\tau = 1$. The resulting gain in computational speed is significant; for example, with $N_\theta = 12$, the computational cost of the equations of motion is reduced to approximately $12/48 = 0.25$ times for an integration step when $\tau = 0$, and $15/48 = 0.315$ times for an integration step when $\tau = 1$. The benefit of this approach is scalable if a higher-order Runge-Kutta scheme is to be used to improve the integration accuracy as well.

Piecewise Sundman Transformation When involving a controller in the equations of motion, it is preferable to use a fixed-step integrator to avoid numerical issues. On the other hand, integrating the spacecraft motion on elliptical orbits with constant time steps is inefficient, since the rapid dynamics near periapsis necessitates a small time step. In contrast, near apoapsis where the dynamics are slower, larger time steps are preferable. As a remedy, the Sundman transformation provides a regularization scheme, where the time step is adapted based on the angular position along the ellipse.

The idea of the piecewise Sundman transformation is to indirectly apply the well-known transformation of the form

$$dt = cr^n ds \quad (31)$$

while maintaining the ODE in terms of time derivatives. The resulting algorithm can still utilize a fixed-step Runge-Kutta scheme, while the actual step size of integration in the time domain is adjusted accordingly. We begin by assigning a fixed angular step size Δs . Given the current semi-major axis a_0 , eccentricity e_0 , and true anomaly f_0 , the current eccentric anomaly of the spacecraft as E_0 , given by

$$\tan \frac{E_0}{2} = \sqrt{\frac{1 - e_0}{1 + e_0}} \tan \frac{f_0}{2} \quad (32)$$

The time-step Δt should be chosen such that the spacecraft's eccentric anomaly at the next time-step is given by $E_1 = E_0 + \Delta s$. For E_0 and E_1 , the corresponding mean anomalies M_0 and M_1 are given by

$$M_i = E_i - e_0 \sin E_i, \quad i = 1, 2 \quad (33)$$

Note that here, we assume e_0 remains constant across the integration step; this approximation holds as the perturbations only act slowly on the state of the spacecraft.

Then, at each step of the integration, the time-step of the integration is chosen at each step of the integration as

$$\Delta t(\Delta s) = \begin{cases} \left(\frac{M_1}{2\pi} - \frac{M_0}{2\pi} \right) P_0 & M_1 > M_0 \\ \left(\frac{M_1}{2\pi} + 1 - \frac{M_0}{2\pi} \right) P_0 & M_1 < M_0 \end{cases} \quad (34)$$

where $P_0 = 2\pi\sqrt{a_0^3/\mu}$ is the period of the orbit at the current time. Again, it is assumed that the a_0 remains constant across the integration step. The two cases in equation (34) is required because $M_0, M_1 \in [0, 2\pi]$. Algorithm 1 summarizes a single integration step using the economic evaluation of equations of motion and the piecewise Sundman transformation.

Algorithm 1 Integration step in custom RK4 scheme

Require: $t_k, \mathbf{x}_k, \Delta s$

$E_0 \leftarrow$ equation (32)

$E_1 \leftarrow E_0 + \Delta s$

Convert E_0 and E_1 to M_0, M_1 via equation (33)

$\Delta t \leftarrow$ equation (34)

$\mathbf{k}_1 \leftarrow$ regular equations of motion at time t_k and state \mathbf{x}_k

$\mathbf{k}_2 \leftarrow$ economic equations of motion at time $t_k + \Delta t/2$ and state $\mathbf{x}_k + (\Delta t/2)\mathbf{k}_1$

$\mathbf{k}_3 \leftarrow$ economic equations of motion at time $t_k + \Delta t/2$ and state $\mathbf{x}_k + (\Delta t/2)\mathbf{k}_2$

$\mathbf{k}_4 \leftarrow$ economic equations of motion at time $t_k + \Delta t$ and state $\mathbf{x}_k + (\Delta t)\mathbf{k}_3$

$\mathbf{x}_{k+1} \leftarrow$ RK4 update via equation (30)

Algorithmic Procedure

To implement Q-law, the ODE corresponding to the Gauss planetary equations must first be implemented. At its core, the ODE function takes in the current state $[\alpha, m]$ and returns the derivative of the states $[\dot{\alpha}, \dot{m}]$ at time t . This ODE is used within a generic initial value problem (IVP) solver as the dynamics to be integrated. While an IVP is solved over some time-span (t_0, t_f) , the integration must be terminated prematurely if the orbital elements converge, or if the propellant of the spacecraft depletes. For this purpose, event functions are used. Event functions can effectively check for the occurrence of user-defined ‘‘events’’ based on a true/false boolean, and trigger user-defined actions, such as the premature termination of the integration. Two events, one checking for convergence and the other checking for propellant depletion, are defined as follows:

$$\text{check}_{\text{convergence}} = \begin{cases} 1 & |W_{\tilde{\alpha}}(\tilde{\alpha} - \tilde{\alpha}_T)| \leq \text{tol}_{\tilde{\alpha}} \quad \forall \tilde{\alpha} \\ 0 & \text{otherwise} \end{cases} \quad (35)$$

$$\text{check}_{\text{propellant}} = \begin{cases} 1 & m(t) < m_{\min} \\ 0 & m(t) \geq m_{\min} \end{cases} \quad (36)$$

where $\text{tol}_{\tilde{\alpha}}$ are the tolerances on convergence along each slow Keplerian element, set to 0.005.

MULTIOBJECTIVE OPTIMIZATION PROBLEM FORMULATION

In order to characterize low-thrust transfers from NRHO to LLO, we formulate a multiobjective optimization problem that embeds Q-law within to evaluate both the transfer time and fuel cost. Furthermore, the spacecraft parameters, namely the initial mass m_0 , maximum thrust c_1 , and I_{sp} are varied as hyper-parameters to this problem.

The multiobjective problem aims to maximize the final mass m_f and minimize the transfer time Δt , and is given by

$$\min_{\mathbf{X}} (-m_f, \text{TOF}) \quad (37)$$

The decision vector \mathbf{X} for a free-epoch problem is given by

$$\mathbf{X} = \left[t_{0,x} \quad t_{0,y} \quad \frac{W_e}{W_a} \quad \frac{W_i}{W_a} \quad W_p \quad k_{r_p} \quad \eta_{a \min, 1} \quad \eta_{a \min, 2} \quad \eta_{r \min, 1} \quad \eta_{r \min, 2} \quad \mathcal{E}_{\text{thres}} \right] \quad (38)$$

If the departure epoch is fixed, the first two variables $t_{0,x}$ and $t_{0,y}$ are removed from \mathbf{X} . Bounds on each value of the decision vector are given in Table 2. Here, $t_{0,x} \in [-1, 1]$ and $t_{0,y} \in [-1, 1]$ denote the departure time from the NRHO, expressed in terms of phase angles, such that the departure time t_0 is given by

$$t_0 = \begin{cases} \frac{\text{atan2}(t_{0,y}, t_{0,x})}{2\pi} \times P_{\text{NRHO}} & \text{atan2}(t_{0,y}, t_{0,x}) \geq 0 \\ \frac{2\pi + \text{atan2}(t_{0,y}, t_{0,x})}{2\pi} \times P_{\text{NRHO}} & \text{atan2}(t_{0,y}, t_{0,x}) < 0 \end{cases} \quad (39)$$

While the use of $t_{0,x}$ and $t_{0,y}$ increases the dimension of the problem, it provides a way to encapsulate the periodicity of the t_0 variable without any discontinuity. Algorithm 2 summarizes the evaluation of the two objectives (37).

Algorithm 2 Fitness function for low-thrust NRHO to LLO transfer

Require: $\mathbf{X}, \mathbf{x}_{\mathcal{R},0}, \tilde{\alpha}_T, m_0, c_1, c_2, \Delta t_{\max}, r_{p \min}$

```

 $\mathbf{x}_{\mathcal{R}}(t_0) \leftarrow \text{ivp}(\mathbf{x}_{\mathcal{R},0}, t_0)$  ▷ Propagate NRHO state in CR3BP
 $\mathbf{x}_{\mathcal{I}}(t_0) \leftarrow \mathbf{C}(\psi)\mathbf{x}_{\mathcal{R}}(t_0)$  ▷ Inertialize state
 $\alpha_0 \leftarrow \text{cart2kep}(\mathbf{x}_{\mathcal{I}}(t_0))$  ▷ Convert to Keplerian elements
 $\lambda_{\oplus,0} \leftarrow \pi + n_{\oplus,G} \left( t_0 \frac{\text{TUC}}{\text{TUG}} \right)$  ▷ Initialize Earth angular position
 $[m_f, \Delta t, \text{converged}] \leftarrow \text{Q-law}(\alpha_0, \tilde{\alpha}_T, m_0, c_1, c_2, \Delta t_{\max}, \mathbf{X}, \lambda_{\oplus,0})$  ▷ Solve Q-law
if converged then
    return  $[-m_f, \Delta t]$  ▷ Return objectives
else
    return  $[1e12, 1e12]$  ▷ Return large penalty
end if

```

RESULTS

The presented Q-law algorithm and optimization problem are deployed to study low-thrust transfers from NRHO to LLOs. Before exploring the design space of the transfers, we begin by evaluating the performance of the customized integration scheme against a conventional, adaptive-step

Table 2. Bounds on optimization variables

Variables	Lower bound	Upper bound
$t_{0,x}, t_{0,y}$	-1.	1.
W_e/W_a	0.1	1.5
W_i/W_a	0.1	1.5
W_P	0.05	0.3
k_{r_p}	1.	50
$\eta_{a \text{ min}, 1}$	0.	0.4
$\eta_{a \text{ min}, 2}$	0.	0.5
$\eta_{r \text{ min}, 1}$	0.	0.02
$\eta_{r \text{ min}, 2}$	0.	0.05
$\mathcal{E}_{\text{thres}}$	-0.5	-0.02

Table 3. Hyper-parameters of the spacecraft, dynamics, and Q-Law

Hyper-parameter	Values
Spacecraft configuration (m_0, c_1, I_{sp}), (kg, N, s)	(1500, 0.4, 2500)
$r_{p \text{ min}}$, km	1738
g_0 , m/s ²	9.81
J_2	202.7×10^{-6}
R_2 , km	1737
Weights on a , Ω and ω [W_a, W_Ω, W_ω]	[1.0, 0.0, 0.0]
$S_{\tilde{\alpha}}$ Parameters, [σ, ν, ζ]	[3, 4, 2]
Integration angular step size Δs , deg	2
N_θ	12

Runge-Kutta method. Then, we proceed to solve the optimization problems, which are formulated using the Metaheuristics.jl library in Julia.³² Firstly, the departure-phase-free problem, where the departure epoch is part of the variable, is solved. Then, the departure-phase-fixed problem is considered for a grid of departure epochs. Hyper-parameters for the numerical experiments are given in Table 3. The initial conditions and the period of the NRHO in the Earth-Moon rotating frame are given in Table 4.

Integration Scheme Performance

The performance of the customized RK4 integration scheme is evaluated against using an implementation of the RK4 with 5th order step correction. Specifically, the Tsit5 algorithm³³ from the DifferentialEquations.jl package³⁴ is used as a point of comparison.

Firstly, the accuracy of the custom integration scheme is evaluated for various angular step size Δs . To this end, the NRHO to LLO transfer problem is solved using $\eta_{a/r \text{ min}, 1/2} = 0$. A relative and absolute tolerance of 10^{-6} is used for the Tsit5 algorithm. Figure 3 shows the solve time as well as the relative difference in final mass and time of flight obtained from the custom RK4 compared

Table 4. Non-zero initial states and period of the NRHO in the Earth-Moon rotating frame centered at their common barycenter

NRHO parameter	Value
x_0, LU_C	1.0213350196144284
z_0, LU_C	-0.18161940230517748
$\dot{y}_0, (\text{LU}/\text{TU})_C$	-0.10175605810056816
$P_{\text{NRHO}}, \text{TU}_C$	1.502061
$P_{\text{NRHO}}, \text{day}$	6.531529005059

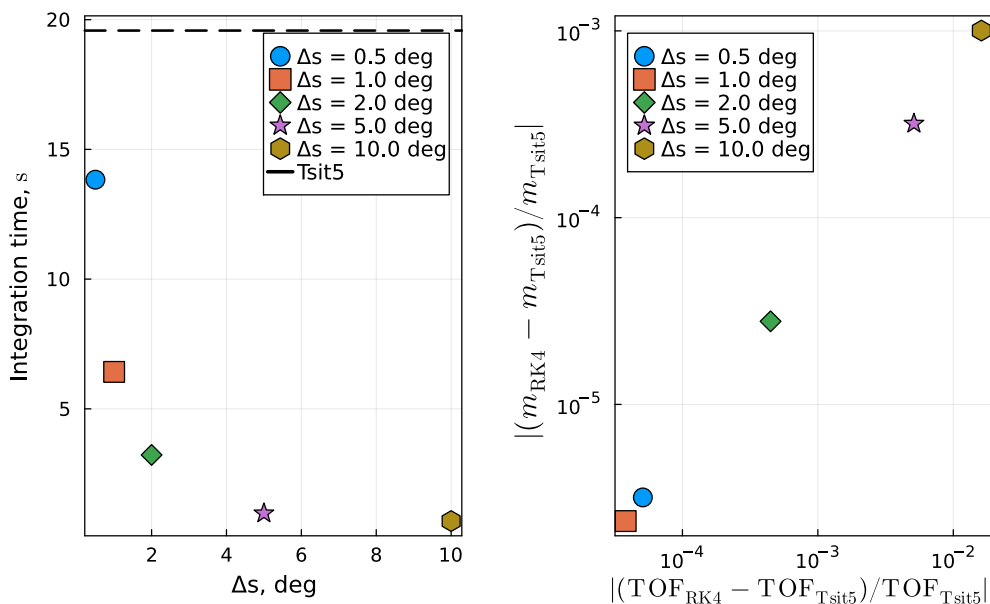


Figure 3. Q-Law solve time and solution accuracy using custom RK4 integrator for varying step-size Δs , compared against adaptive-step integrator (Tsit5)

to Tsit5. As expected, the computational cost of the custom integration scheme reduces drastically as the step size is decreased. Meanwhile, the difference in final mass and time of flight is within fractions of a percent for all cases with step sizes under 10° . In the remainder of this work, we use a step size of $\Delta s = 2^\circ$ as it provides a good trade-off between integration time and error.

Next, the effect of increasing N_θ is tested. This time, the NRHO to LLO transfer problem is solved using $\eta_{a \text{ min}, 1/2} = 0.2$ and $\eta_{r \text{ min}, 1/2} = 0$. For the custom RK4 integrator, a step size of $\Delta s = 2^\circ$ is used, and the tolerances for Tsit5 are set again to 10^{-6} . Figure 4 shows the solve time for various values of N_θ using the two integration schemes. Again, as expected, the solve time grows much slower with the custom RK4; for the same computational budget, we can use larger values of N_θ , hence enabling better approximations of \dot{Q}_{nn} and \dot{Q}_{nx} from equations (26) and (27).

Free Departure Phase Angle

We first consider the multiobjective problem with free departure epoch. This enables us to discover the optimal departure location along NRHO for the type of low-thrust transfers considered in

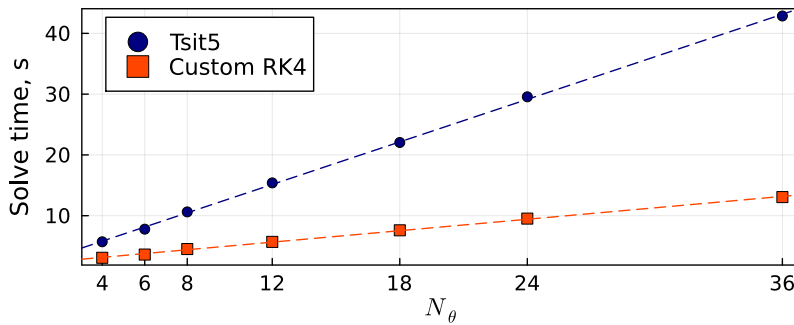


Figure 4. Q-Law solve time using adaptive-step integrator (Tsit5) and custom RK4 integration scheme with step size $\Delta s = 2^\circ$

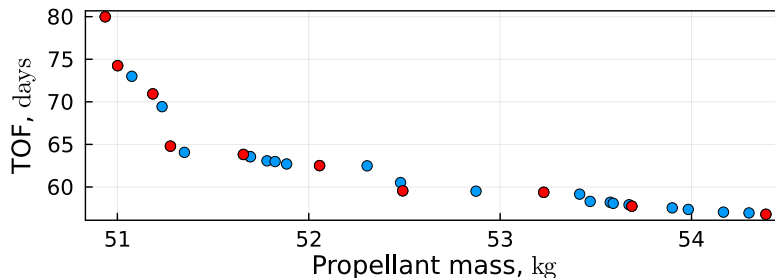


Figure 5. Pareto solutions from free departure epochs. Red markers indicate selected representative solutions for further analysis.

this work. Figure 5 shows the Pareto front discovered through the method presented thus far. Along the detected Pareto front, a variation in time of flight of about 20 days has been observed, for a propellant mass trade-off of 5 kg.

Insight can also be drawn by looking at the spacecraft trajectory in terms of osculating Keplerian elements with respect to the Moon. This is shown in Figure 7 for a select number of solutions along the Pareto front. It is possible to see that the Pareto solutions initially prioritize reduction in semi-major axis, followed by reduction in eccentricity as well. This follows the need for the spacecraft to initially reduce its energy in order to get fully-captured by the Moon.

Fixed Departure Phase Angle

We now bring our attention to the fixed departure epoch cases. We consider a departure epoch grid $t_0 \in [0, P_{\text{NRHO}})$ discretized by 60. This allows us to obtain an analog to pork-chop plots, a useful “map” for mission planners to determine the trajectory options concurrently with other operational or programmatic constraints. Figure 8 shows the Pareto solutions solved over multiple instances, where in each instance the departure is fixed to a specific time along the NRHO.

It is possible to observe that leaving at perilune results in overall higher propellant cost. This may seem counter-intuitive when considering two-body transfers, as in a two-body setting, the reduction of energy is most efficiently done at perilune. However, the presence of strong perturbation force, as well as the Lyapunov function’s penalty term on the periapsis (17), renders it a not-as-attractive starting location. Coincidentally, the region near perilune also coincides with the portion of the NRHO that is known to be highly sensitive, and therefore to be avoided for proximity operation

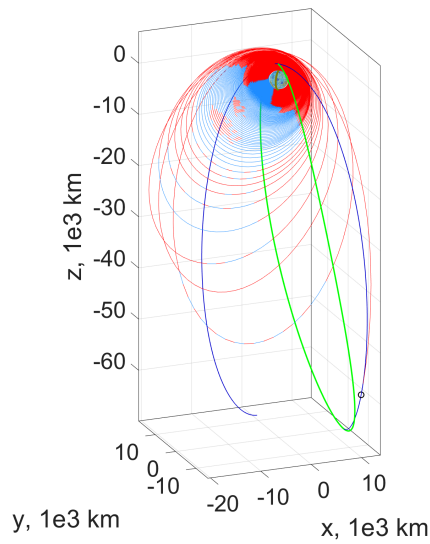


Figure 6. Example NRHO to Low-Thrust Transfer with departure phase angle $t_0 = 0.2P_{\text{NRHO}}$. The lime green line is the NRHO in the Earth-Moon rotating plane defined at $t_0 = 0$, and the black line is the NRHO in the inertial frame. The red and blue arcs represent thrusting and coasting arcs along the transfer, respectively.

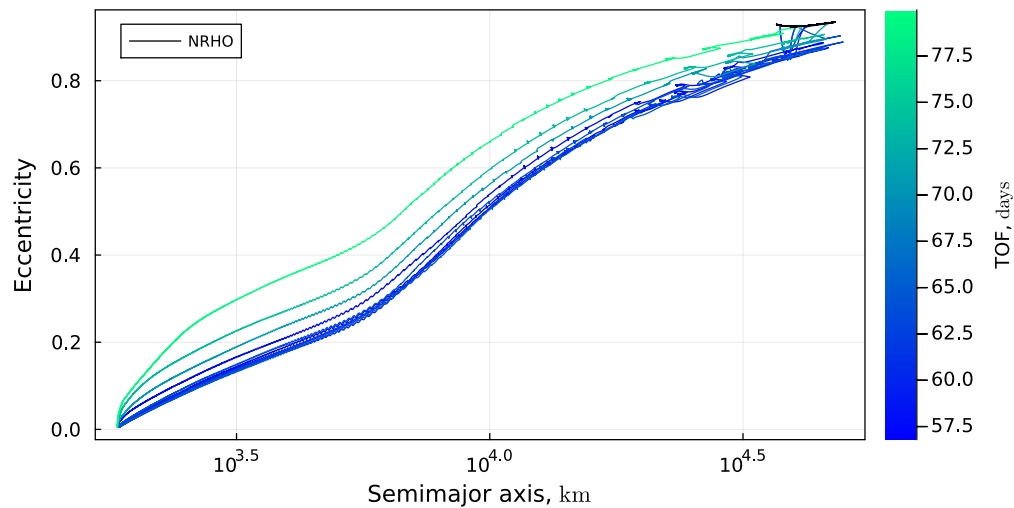


Figure 7. a - e history for selected free-epoch Pareto solutions

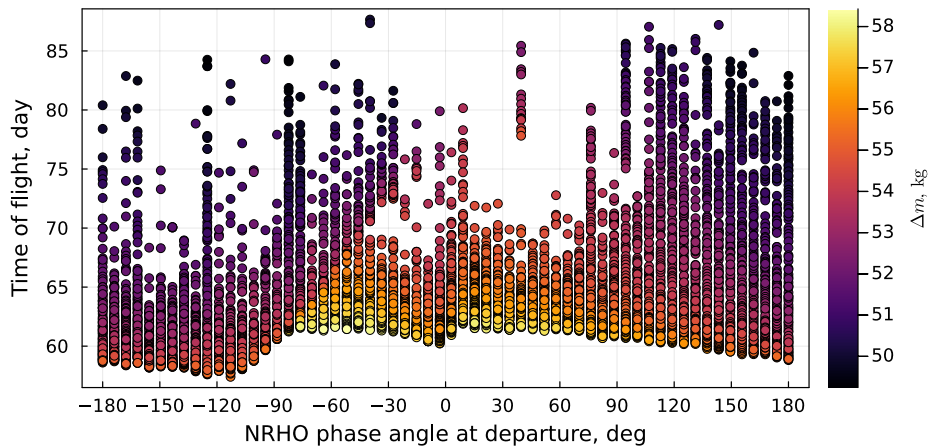


Figure 8. Pareto solutions from fixed departure epochs along NRHO. A phase angle of 0° corresponds to perilune, and a phase angle of $\pm 180^\circ$ corresponds to apolune.

with the Gateway.³⁵

The shortest time-of-flight coincides to a departure angle of around -120° , or 60° from apolune. Meanwhile, solutions with low-propellant mass are available across most of the departure epoch. This is a simple consequence that, given a long enough loitering time along the transfer, near-mass-optimal orbit transfers can be found regardless of the departure phase. As an exception, fewer propellant-conserving solutions are observed for departure phase angles of between -30° to about 60° . This is reflective of the aforementioned high sensitivity of the dynamics around perilune, where starting the low-thrust transfer going into this portion of the NRHO is more likely to be disturbed out of the cislunar vicinity when using the feedback controller.

CONCLUSION

In this work, we developed a customized Q-law algorithm for designing many-revolution low-thrust transfers from the Gateway’s baseline NRHO to LLOs. The Lyapunov controller is designed to deduce a control based solely on two-body dynamics, while perturbations are added into the dynamics used for propagating the spacecraft state. To incorporate coasting mechanisms efficiently, a custom Runge-Kutta scheme with an economic evaluation of the coasting heuristics and a piecewise Sundman Transformation is implemented. The resulting algorithm can compute the many-revolution transfer within a few seconds, rendering itself well for large-scale trade-study.

This formulation is used within a dual objective optimization problem to design fuel and time of flight efficient transfers. Specifically, the optimization problem is solved with a free departure phase angle scenario and a grid-based fixed phase angle scenario. Pareto solutions trading off propellant mass and time of flight have been uncovered for a plausible cislunar low-thrust transfer vehicle. The obtained trends can be further analyzed through transfer designs in higher-fidelity models, while also providing crucial insights into the feasibility of low-thrust-based space transportation architecture in the NRHO-LLO interval.

REFERENCES

- [1] G. Chavers, N. Suzuki, M. Smith, L. Watson-Morgan, S. W. Clarke, W. C. Engelund, L. Aitchison, S. McEniry, L. Means, M. DeKlotz, and S. Jackson, “NASA’s Human Lunar Landing Strategy,” 2019, pp. 1–6.
- [2] D. J. Israel, K. D. Mauldin, C. J. Roberts, J. W. Mitchell, A. A. Pulkkinen, L. V. D. Cooper, M. A. Johnson, S. D. Christe, and C. J. Gramling, “LunaNet: A Flexible and Extensible Lunar Exploration Communications and Navigation Infrastructure,” *IEEE Aerospace Conference Proceedings*, 2020, 10.1109/AERO47225.2020.9172509.
- [3] S. L. Mccarty, W. K. Sjauw, L. M. Burke, and M. L. Mcguire, “Analysis of Near Rectilinear Halo Orbit Insertion with a 40-kW Solar Electric Propulsion System,” 2018.
- [4] R. E. Pritchett, E. M. Zimovan, and K. C. Howell, “Impulsive and low-thrust transfer design between stable and nearly-stable periodic orbits in the restricted problem,” *AAS Space Flight Mechanics Meeting*, No. 210009, 2018, 10.2514/6.2018-1690.
- [5] R. J. Whitley, D. C. Davis, L. M. Burke, B. P. Mccarthy, R. J. Power, M. L. Mcguire, and K. C. Howell, “Earth-Moon Near Rectilinear Halo and Butterfly Orbits for Lunar Surface Exploration,” 2018.
- [6] D. C. Davis, K. K. Boudad, S. M. Phillips, and K. C. Howell, “Disposal, Deployment, and Debris in Near Rectilinear Halo Orbits,” 2019.
- [7] D. E. Lee, “National Aeronautics and Space Administration (NASA) White Paper: Gateway Destination Orbit Model: A Continuous 15 Year NRHO Reference Trajectory,” 2019.
- [8] C. Du and O. L. Starinova, “Orbital perturbation analysis and generation of nominal near rectilinear halo orbits using low-thrust propulsion,” Vol. 236, 2019, pp. 2974–2990, 10.1177/09544100211072318.
- [9] Astroscale, “Astroscale to Advance On-Orbit Servicing Interface Technologies Supported by Latest Award from Japanese National Research and Development Agency,” 2022.
- [10] Spaceflight, “Sherpa Program: New Orbital Transfer Vehicles Launch Smallsats to Custom Orbital Destinations,” 2022.
- [11] “Low-thrust transfer design based on collocation techniques: Applications in the restricted three-body problem,” Vol. 162, 2017, pp. 299–318.
- [12] “Extended mission options for the lunar icecube low-thrust spacecraft by leveraging the dynamical environment,” *Proceedings of the International Astronautical Congress, IAC*, Vol. 2020-October, No. October, 2020, pp. 12–14.
- [13] A. Das-Stuart, K. C. Howell, and D. C. Folta, “Rapid trajectory design in complex environments enabled by reinforcement learning and graph search strategies,” *Acta Astronautica*, Vol. 171, 6 2020, pp. 172–195, 10.1016/j.actaastro.2019.04.037.
- [14] Y. Kayama, K. C. Howell, M. Bando, and S. Hokamoto, “Low-Thrust Trajectory Design with Successive Convex Optimization for Libration Point Orbits,” *Journal of Guidance, Control, and Dynamics*, 2022, pp. 1–15, 10.2514/1.g005916.
- [15] J. F. Horton, T. Kokan, C. R. Joyner, D. Morris, and R. Noble, “Lunar landing and sample return from near rectilinear halo orbit using high-powered solar electric propulsion,” *AAS Annual Guidance and Control Conference*, Vol. 169, 2019, pp. 487–497.
- [16] B. Park, K. C. Howell, and D. C. Folta, “Design of Low-Thrust Transfers from an NRHO to Low Lunar Orbits: Applications for Small Spacecraft,” *AAS/AIAA Astrodynamics Specialist Conference*, 2021.
- [17] A. E. Petropoulos, “Simple Control Laws for Low-Thrust Orbit Transfers,” *AAS/AIAA Astrodynamics Specialists Conference*, 2003.
- [18] A. E. Petropoulos, “Low-thrust orbit transfers using candidate Lyapunov functions with a mechanism for coasting,” *AIAA/AAS Astrodynamics Specialist Conference*, No. August, 2004, 10.2514/6.2004-5089.
- [19] A. E. Petropoulos, “Refinements to the Q-law for low-thrust orbit transfers,” *AAS/AIAA Space Flight Mechanics Meeting*, 2005.
- [20] G. I. Varga and J. M. S. Perez, “Many-Revolution Low-Thrust Orbit Transfer Computation Using Equinoctial Q-Law Including J2 and Eclipse Effects,” *ICATT*, No. 1, 2016.
- [21] R. Epenoy and D. Pérez-Palau, “Lyapunov-based low-energy low-thrust transfers to the Moon,” *Acta Astronautica*, Vol. 162, No. December 2018, 2019, pp. 87–97, 10.1016/j.actaastro.2019.05.058.
- [22] J. L. Shannon, M. T. Ozimek, J. A. Atchison, and C. M. Hartzell, “Q-law aided direct trajectory optimization of many-revolution low-thrust transfers,” *Journal of Spacecraft and Rockets*, Vol. 57, No. 4, 2020, pp. 672–682, 10.2514/1.A34586.
- [23] H. Holt, R. Armellin, N. Baresi, Y. Hashida, A. Turconi, A. Scorsoglio, and R. Furfaro, “Optimal Q-laws via reinforcement learning with guaranteed stability,” *Acta Astronautica*, Vol. 187, No. March, 2021, pp. 511–528, 10.1016/j.actaastro.2021.07.010.

- [24] M. Wijayatunga, R. Armellin, H. Holt, L. Pirovano, and A. A. Lidtke, “Design and Guidance of a Multi-Active Debris Removal Mission,” 2022, 10.48550/ARXIV.2210.11701.
- [25] B. B. Jagannatha, J. B. H. Bouvier, and K. Ho, “Preliminary design of low-energy, low-thrust transfers to halo orbits using feedback control,” *Journal of Guidance, Control, and Dynamics*, Vol. 42, No. 2, 2019, pp. 260–271, 10.2514/1.G003759.
- [26] D. Ottesen and R. P. Russell, “Piecewise Sundman Transformation for Spacecraft Trajectory Optimization Using Many Embedded Lambert Problems,” *Journal of Spacecraft and Rockets*, Vol. 59, No. 4, 2022, pp. 1044–1061, 10.2514/1.A35140.
- [27] E. M. Zimovan, *Near Rectilinear Halo Orbits Within the Earth-Moon System*. PhD thesis, 2017.
- [28] C. Thangavelu, *Transfers between Near Rectilinear Halo Orbits and Low Lunar Orbits*. PhD thesis, 2019.
- [29] R. Whitley and R. Martinez, “Options for staging orbits in cislunar space,” *IEEE Aerospace Conference Proceedings*, 2015, 10.1109/AERO.2016.7500635.
- [30] E. M. Zimovan, K. C. Howell, and D. C. Davis, “Near rectilinear halo orbits and their application in Cis-Lunar space,” *3rd IAA Conference on Dynamics and Controls of Space Systems*, Vol. 161, 2017, pp. 209–228.
- [31] H. Li, S. Chen, and H. Baoyin, “J2-perturbed multitarget rendezvous optimization with low thrust,” *Journal of Guidance, Control, and Dynamics*, Vol. 41, 2018, pp. 796–802, 10.2514/1.G002889.
- [32] J.-A. M. d. Dios and E. Mezura-Montes, “Metaheuristics: A Julia Package for Single- and Multi-Objective Optimization,” *Journal of Open Source Software*, Vol. 7, No. 78, 2022, p. 4723, 10.21105/joss.04723.
- [33] C. Tsitouras, “Runge–Kutta pairs of order 5(4) satisfying only the first column simplifying assumption,” *Computers Mathematics with Applications*, Vol. 62, No. 2, 2011, pp. 770–775, <https://doi.org/10.1016/j.camwa.2011.06.002>.
- [34] C. Rackauckas and Q. Nie, “DifferentialEquations.jl—a performant and feature-rich ecosystem for solving differential equations in Julia,” *Journal of Open Research Software*, Vol. 5, No. 1, 2017.
- [35] D. Guzzetti, E. M. Zimovan, K. C. Howell, and D. C. Davis, “Stationkeeping Analysis for Spacecraft in Lunar Near Rectilinear Halo Orbits,” 2017.